Journal of Catalysis 364 (2018) 271–281

Contents lists available at ScienceDirect

Journal of Catalysis

journal homepage: www.elsevier.com/locate/jcat

High performance V_2O_5/MgF_2 catalysts for gas-phase dehydrofluorination of 1,1,1,3,3-pentafluoropropane: Support-induced evolution of new active sites

Jian-Dong Song, Tong-Yang Song, Ting-Ting Zhang, Yun Wang, Meng-Fei Luo *, Ji-Qing Lu *

Key Laboratory of the Ministry of Education for Advanced Catalysis Materials, Institute of Physical Chemistry, Zhejiang Normal University, Jinhua 321004, China

ARTICLE INFO

Article history:
Received 13 December 2017
Revised 10 April 2018
Accepted 11 April 2018
Available online 15 June 2018

Keywords:
V_2O_5/MgF_2
HFC-245fa
Dehydrofluorination
HFO-1234ze
Vanadium oxyfluoride

ABSTRACT

A series of supported V_2O_5/MgF_2 catalysts were prepared and tested for dehydrofluorination of 1,1,1,3,3-pentafluoropropane (HFC-245fa) to synthesize 1,3,3,3-tetrafluoropropene (HFO-1234ze). The addition of V_2O_5 in MgF_2 resulted in up to 5-fold increase in HFC-245fa conversion (from 19.2 to 95.2%) and much enhanced catalyst stability. Characterization results revealed that the dehydrofluorination initiated on the MgF_2 support triggered the transformation of V_2O_5 to vanadium oxyfluoride (VOF_x) species via the reaction between V_2O_5 and HF, and such species were responsible for the improved activity as they had much higher turnover frequencies (TOFs) than the MgF_2 (0.762 s^{-1} v.s. 0.026 s^{-1} at 320 °C). The kinetic results indicated that the $3.1V_2O_5/MgF_2$ had much lower activation energy (44.6 ± 1.9 kJ mol^{-1}) than the MgF_2 (69.0 ± 0.8 kJ mol^{-1}). Accordingly, reaction mechanism on the V_2O_5/MgF_2 catalyst was proposed, which included slow dehydrofluorination on MgF_2 and fast dehydrofluorination on the VOF_x species.

1. Introduction

Hydrofluorocarbons (HFCs) such as 1,1,1,2-tetrafluoroethane (HFC-134a) have been widely used as refrigerant and blowing agent, but the production and consumption of HFCs would be reduced in phases according to the Montreal Protocol, due to their high global warming potentials (GWP) [1,2]. Alternatively, hydrofluoroolefins (HFOs) containing highly reactive C=C double bond have advantages such as short atmospheric life time, zero ozone depletion potential (ODP) and low global warming potential (GWP). Among these HFO compounds, 2,3,3,3-tetrafluoropropene (HFO-1234yf) and 1,3,3,3-tetrafluoropropene (HFO-1234ze) have excellent environmental parameters such as high refrigeration efficiency and good compatibility and thus are regarded as potential candidates for the replacement of HFC-134a [3,4].

One promising route for the synthesis of HFO-1234ze is dehydrofluorination of 1,1,1,3,3-pentafluoropropane (HFC-245fa) because it consumes HFC-245fa with high GWP (GWP = 858). For catalytic reactions involving HF (such as dehydrofluorination and chlorine/fluorine exchange reaction), metal oxides and metal fluorides have been used as catalysts and/or supports due to their good stability under corrosive environment [5–7]. In addition to the well-known Cr-based catalysts [8–11], compounds such as SbF_5 [12] and AlF_3 [13,14] with strong surface acidity are active for dehydrofluorination because it has been well recognized that the surface acid sites are responsible for the activation of C—F bond during dehydrofluorination [15]. For example, it was reported by Teinz et al. [16] that the dehydrofluorination of 3-chloro-1,1,1,3-tetrafluorobutane took place on the strong Lewis acid sites in the AlF_3 catalyst. Recently, it was found that high surface area Nano α-AlF_3 with strong surface acidity was very active for dehydrofluorination of various hydrofluorocarbons [17]. However, the side effect of such strong acidity is the formation of coke or polymer on the catalyst surface, which results in rapid catalyst deactivation [18]. Li et al. [19] reported that the active sites for CF_2CH_2 formation were weak acid sites on the $Mg_2P_2O_7$ catalysts for the dehydrofluorination of CF_3CH_3 and carbon deposition and polymerization took place on strong acid sites. Therefore, it seems that materials with medium surface acidity and robustness in corrosive environment (because of the production of HF) could be promising candidates as stable catalyst systems for dehydrofluorination reaction. MgF_2 with good thermal stability has been reported as a support for a number of transition metal oxides. Although the acidity of MgF_2 itself is very weak, it could be improved by the modification of aliovalent cations (such as V, Fe, Cr) in MgF_2 [20–22]. Kemnitz et al. [20] found that Lewis acidity was not detectable in pure MgF_2, but it increased significantly with the MgF_2/VF_3 samples. Vana-

* Corresponding authors.
E-mail addresses: mengfeiluo@zjnu.cn (M.-F. Luo), jiqinglu@zjnu.cn (J.-Q. Lu).

https://doi.org/10.1016/j.jcat.2018.04.014
0021-9517/

dium oxide is a versatile catalyst for various reactions such as oxidative dehydrogenation of propane [23] and it possesses considerable surface acidity [24]. When vanadium oxide was supported on MgF_2, it was reported that the acidic properties of the catalyst were not the sum of the acidities of its components but were formed in the process of interaction between vanadium species and the support [25].

Thus, in the current work, gas phase dehydrofluorination of HFC-245fa was performed on a series of supported V_2O_5/MgF_2 catalysts. The first goal of this work is to seek stable catalysts for this reaction, and it turns out that the addition of V_2O_5 could remarkably enhance the catalytic performance (higher activity and better stability) compared to the MgF_2 support. The second goal is to identify the active sites of the catalyst. It is well known that for dehydrofluorination reaction, possible phase change must be considered because metal oxide could easily react with HF to form metal oxyfluoride or metal fluoride (particularly at high reaction temperatures), which would alter the catalyst nature and consequently the catalytic behaviors. One example is the formation of active chromium oxyfluoride species on the Cr-based catalysts during the F/Cl exchange reaction [26,27]. In the current work, support-induced generation of new active species (VOF_x) was observed, based on various characterizations of the catalysts. Such species were found to be much more active than the MgF_2 support, which was evidenced by kinetic investigation on the representative catalysts.

2. Experimental

2.1. Catalyst preparation

$La(NO_3)_3{\cdot}6H_2O$, $Y(NO_3)_3{\cdot}6H_2O$, $Ni(NO_3)_2{\cdot}9H_2O$ and $Fe(NO_3)_3{\cdot}9H_2O$ were purchased from Sinopharm Group Chemical Reagent Co., Ltd.; NH_4VO_3, $In(NO_3)_3{\cdot}9H_2O$ and $Ga(NO_3)_3{\cdot}9H_2O$ were purchased from Shanghai Macklin Biochemical Technology Co., Ltd.; All the chemicals were of analytic grade purity and were used as received without further purification. The MgF_2 (purity of 97.5%) support was purchased from Shanghai Aladdin Biochemical Technology Co., Ltd.

The supported catalysts were prepared by an impregnation method. Taking NiO/MgF_2 as an example, a detailed process was as follows: an aqueous solution containing 0.236 g $Ni(NO_3)_2{\cdot}6H_2O$ (0.81 mmol) was mixed with 5 g MgF_2 (80.25 mmol) at room temperature for 4 h. Then the excess water was evaporated at 80 °C and the solid was dried at 100 °C overnight. Finally, the resulting solid was calcined at 400 °C for 4 h in static air to obtain the catalyst, which was denoted as $1.0NiO/MgF_2$ (the number 1.0 means that the Ni molar percentage per mole MgF_2 is 1.01%). Catalysts with other supported transition metal oxides were prepared in a similar manner, with a metal percentage per mole MgF_2 of 1.01%. The V_2O_5/MgF_2 catalysts with different V_2O_5 contents were also prepared in a similar manner. The catalysts with V molar percentages per mole MgF_2 of 1.0, 3.1, 6.4 and 9.9% were denoted as $1.0V_2O_5/MgF_2$, $3.1V_2O_5/MgF_2$, $6.4V_2O_5/MgF_2$ and $9.9V_2O_5/MgF_2$, respectively. The reference pure V_2O_5 catalyst was prepared by thermal decomposition (400 °C for 4 h in static air, at a ramp of 10 °C min^{-1} from room temperature to 400 °C) of ammonium metavanadate (NH_4VO_3).

2.2. Catalyst characterizations

Surface areas of the catalysts were determined by the modified BET method from N_2 adsorption isotherms at liquid nitrogen temperature (−195.7 °C) on a NOVA 4000e Surface Area & Pore Size Analyzer. Before the measurements, the samples were outgassed at 200 °C for 4 h under vacuum.

The X-ray diffraction (XRD) patterns of the catalysts were determined with a X'pert PRO MPD PW 3040/60 powder diffractometer using Cu Kα radiation. The working voltage was 40 kV and the working current was 40 mA. The patterns were collected in a 2θ range from 10 to 70° with a scanning speed of 0.3° s^{-1}.

The Raman spectra of the catalysts were collected on a Renishaw Invia confocal microprobe under ambient condition (laser power = 3 mW, dwell time = 60 s, number of scans = 4, resolution = 1 cm^{-1}). The wavelength of the excitation laser was 325 nm. Before the measurement, the sample was heated under a infrared lamp (80 °C, 15 min) to remove water in the sample.

Surface acidity of the catalysts was measured by ammonia temperature programmed desorption (NH_3-TPD) which was carried out in a home-made fixed-bed reactor (i. d. =6 mm) containing 80 mg of catalyst. The sample was heated from 30 to 300 °C at a rate of 10 °C min^{-1}, kept at 300 °C for 30 min and cooled down to 50 °C in a flow of N_2 (30 ml min^{-1}). Then a flow of NH_3 (30 ml min^{-1}) was introduced to the reactor for 30 min. The gaseous or physically adsorbed NH_3 was removed by purging with N_2 flow (30 ml min^{-1}) at 100 °C for 30 min. Then the sample was heated in the N_2 flow from 50 to 800 °C at a rate of 20 °C min^{-1}, and the profile was recorded using a mass spectrometer (Omnistar-200) monitoring m/e = 17.

X-ray photoelectron spectra (XPS) of the catalysts were obtained on an ESCALAB 250Xi instrument, with a Al Kα X-ray source (1486.6 eV), under about 2×10^{-9} mbar at room temperature and a pass energy of 20 eV. The binding energy of F1s core level at 685.5 eV was taken as the internal standard.

The Fourier transform infrared (FTIR) spectra of the catalysts were recorded on a NEXUS670 spectrometer. The catalysts were pressed to a self-supported wafer (about 20 nm, with a diameter of 16 mm) and the spectra were recorded at room temperature. Before the measurement, the sample was heated under a infrared lamp (80 °C, 15 min) to remove water in the sample.

In situ Fourier transform infrared (FTIR) spectroscopy of pyridine adsorption was performed on a Bruker TENSOR 27 FTIR spectrometer. About 16 mg of the sample was pressed into a 13 mm self-supported wafer and placed into an in situ IR cell. The sample was then heated from room temperature to 350 °C at a rate of 10 °C min^{-1} under vacuum. The sample was kept at 350 °C for 2 h and then cooled to room temperature, and then it was exposed to pyridine vapor for 10 min at room temperature. Then it was purged at 150 °C for 30 min in a He flow, followed by the spectrum recording in the range of 1200–1700 cm^{-1} with 32 scans and at a resolution of 4 cm^{-1}.

2.3. Catalytic testing and kinetic study

The catalytic performance test was carried out in a stainless steel tubular reactor (10 mm (i.d.) × 300 mm) under atmospheric pressure. 0.8 g of the catalyst (40–60 mesh, with a volume of about 1 ml) was loaded into the reactor with a thermal couple placed in the middle of the catalyst bed to monitor the reaction temperature. The catalyst was pretreated in a N_2 flow (30 ml min^{-1}) at 300 °C for 30 min. Then the N_2 flow was stopped and a mixture of N_2 and HFC-245fa with a flow ratio of HFC-245fa/N_2 = 3.2/10.8 ml min^{-1} was introduced (total flow = 14 ml min^{-1}, GHSV = 840 h^{-1}). To remove the product HF, the reaction effluent passed an aqueous KOH solution and then it was analyzed by a gas chromatograph (Shimadzu GC-2014) equipped with a flame ionization detector (FID) and a GS-GASPRO capillary column (0.32 mm × 60 m). Carbon balances were close to 100 ± 3%. The HFC-245fa conversion and product selectivity were defined as follows:

HFC-245fa conversion = mol of all detectable products/mol of HFC-245fa in feed.

Product selectivity = mol of target product/mol of all detectable products.

It should be noted that due to the fact that the effluent passed through an aqueous KOH solution to neutralize HF, the possible hydrolysis of the organic products (trans-HFO-1234ze and cis-HFO-1234ze) might occur and thus the calculated conversion and selectivity might contain deviations. To confirm this, a pre-experiment was conducted. A mixed gas containing pure 20% of trans-HFO-1234ze and 80% of N_2 (total flow rate = 14 ml min^{-1}) passed through the container with aqueous KOH solution (1000 ml) for 4 h, which corresponded a total trans-HFO-1234ze mole of 30 mmol. Then, the solution was analyzed by GC and it was found that in addition to the signal of trans-HFO-1234ze, a new unidentified signal (appeared behind the trans-HFO-1234ze) was detected and the peak area of this signal is about 12% of that of the trans-HFO-1234ze, suggesting that the hydrolysis of trans-HFO-1234ze possibly occurs. Moreover, judging from the peak areas of these two compounds, it could be estimated that the trans-HFO-1234ze content in the 1000 ml container was about 0.54 mmol, which indicated that about 1.8% of the HFO-1234ze could be dissolved in the solution during the neutralization process.

The kinetic study was performed on the same fixed bed reactor. The feed gases were measured with mass flow controllers and mixed prior to the reactor inlet. For kinetic measurements, the reaction was operated in a differential mode with HFC-245fa conversion less than 15%. In typical kinetic tests, the partial pressure of HFC-245a was adjusted by changing the molar ratio of HFC-245a/N_2 while keeping the total flow rate constant. Also, the absence of mass transport limitation was checked by Weisz - Prater criterion for internal diffusion and Mears' criterion for external diffusion and the absence of heat transfer was checked by Mears' criterion [28] (See Supporting Information for detailed calculation). The calculated values ensure plug-flow and isothermal conditions within the catalyst bed. The power-rate law expressions were obtained by taking partial pressure of each reactant (kPa) and the reaction rate data and simultaneously fitting the entire data set by linear least squares regression analysis using the POLYMATH 5.1 program [29].

3. Results and discussion

3.1. Catalytic performance of MO_x/MgF_2 catalysts

Table 1 lists the catalytic performance of the MO_x/MgF_2 catalysts for dehydrofluorination of HFC-245fa. At the reaction temperature of 340 °C, the MgF_2 support gives a medium HFC-245fa conversion of 19.2%, and the addition of La_2O_3, NiO or Y_2O_3 somehow suppresses the activity. In contrast, the addition of In_2O_3, Ga_2O_3, FeO_x or V_2O_5 significantly enhances the activity. Particularly, the addition of 1.0% of V_2O_5 on the MgF_2 improves the activity by 3-fold (67.7%) compared to that of the MgF_2 (19.2%). Concerning the selectivity, all the catalysts show very high selectivity (about 99.8%) to HFO-1234ze. Among the products, it is found that the major product is trans-HFO-1234ze (with a selectivity of about 80%) and the minor product is cis-HFO-1234ze (with a selectivity of about 20%) and very small amount of HFO-1234yf is also produced (with a selectivity of about 0.3%). The screening of various catalysts reveals that the supported V_2O_5/MgF_2 could be a promising candidate for this reaction and thereafter detailed experiments are focused on this system (V_2O_5/MgF_2).

3.2. Characterizations of V_2O_5/MgF_2 catalysts

Fig. 1 shows the XRD patterns of the fresh and spent V_2O_5/MgF_2 catalysts (the spent catalysts refer to those after 1 h reaction). As shown in Fig. 1a, the fresh MgF_2 support shows intensive diffractions at 2θ of 27.2, 35.2, 40.0, 43.7, 53.5, 56.2, 60.7 and 68.1°, which are attributed to crystalline MgF_2 (JCPDS No. 41-1443). After the addition of V_2O_5, these diffractions remain but their intensities gradually decline with increasing V_2O_5 content, indicating that the addition of V_2O_5 somehow suppresses the growth of MgF_2 crystallites. Similar phenomenon was observed on V_2O_5/MgF_2 catalysts by Narayana et al. [30] and was explained by the coverage of MgF_2 by the molecular structures of VO_x. However, this might be not true because the X-ray could penetrate very deep in the sample and the patterns reflect the bulk information. Instead, the declined intensity of the MgF_2 diffractions might be an implication of the possible formation of magnesium vanadates compounds such as $Mg_3(VO_4)_2$, $Mg_2V_2O_7$ or MgV_2O_6 through the reaction between vanadium species and the MgF_2 support [31]. Unfortunately, no noticeable diffractions of such compounds could be detected (e.g. JCPDS No. 37-0351 for $Mg_3(VO_4)_2$, JCPDS No. 31-0816 for $Mg_2V_2O_7$, JCPDS No. 40-0164 for MgV_2O_6), which implies that such magnesium vanadates could be highly dispersed on the surface due to their very low contents in the sample. Indeed, the formation of such compounds usually requires high calcination temperature (e.g. > 600 °C) [31] but in the current work the samples were calcined at rather low temperature (400 °C). Also, the diffractions of V_2O_5 are not observed when the V_2O_5 loading is lower than 3.1%, implying that the VO_x species are highly dispersed at low loadings. However, for the $6.4V_2O_5/MgF_2$ and $9.9V_2O_5/MgF_2$ catalysts, some weak XRD reflection peaks at 2θ of 15.2, 20.3, 21.7, 26.2, 30.9, 34.4, 43.7 and 51.1° are observed, which are assigned to the crystalline V_2O_5 (JCPDS No. 41-1426). The structures of vanadium oxide are related to its content on the support, which has been reported in literature [32–34]. At low vanadium loadings, the main species are isolated VO_4 tetrahedral; while at high loadings, the dominant vanadium species are chains of $(VO_3)_n$, islands of trigonal pyramids or crystalline V_2O_5 [35]. For the spent catalysts, Fig. 1b

Table 1
Catalytic performance of various supported catalysts at reaction temperature of 340 °C.[a]

Catalyst	Conversion/%	Selectivity/%		
		trans-HFO-1234ze	cis-HFO-1234ze	HFO-1234yf
MgF_2	19.2	80.2	19.5	0.3
$1.0In_2O_3/MgF_2$	34.8	80.2	19.6	0.2
$1.0Ga_2O_3/MgF_2$	38.2	81.7	18.1	0.2
$1.0Fe_2O_3/MgF_2$	53.7	82.5	17.2	0.3
$1.0V_2O_5/MgF_2$	67.7	81.1	18.7	0.2
$1.0La_2O_3/MgF_2$	15.8	75.6	24.1	0.3
$1.0NiO/MgF_2$	18.7	75.2	24.5	0.3
$1.0Y_2O_3/MgF_2$	11.5	76.6	23.2	0.2

[a] Data were taken after 1 h reaction.

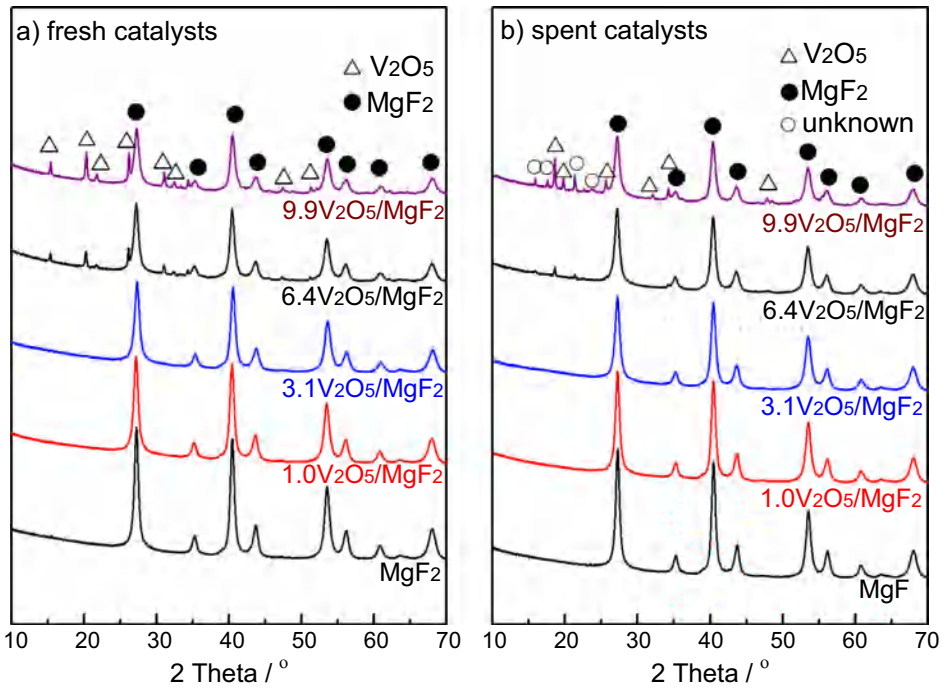

Fig. 1. XRD patterns of (a) fresh and (b) spent V_2O_5/MgF_2 catalysts.

shows that the patterns are generally similar to those of the fresh ones, but two differences are also observed. One is that the diffractions of V_2O_5 oxide become weaker compared to those of the fresh ones. The other is that some new diffractions (2θ = 17.5, 19.7, 21.2 and 23.7°) emerge for the spent $9.9V_2O_5/MgF_2$ catalyst. The appearance of such diffractions suggests the formation of some new vanadium-containing species during the reaction, but unfortunately these diffractions do not match any of known compounds in the XRD diffraction database. Nevertheless, it is reasonable to assume that the evolution of such new species is related to the transformation of V_2O_5 oxide during the reaction, and the nature of such species will be discussed based on the other characterization results.

Fig. 2 shows the Raman spectra of the fresh and spent V_2O_5/MgF_2 catalysts. For the fresh catalysts (Fig. 2a), the distinct bands at 363 cm^{-1} (δ_{V-O}), 530 cm^{-1} ($\delta_{V=O}$) and the broad bands in the 600–1000 cm^{-1} region can ascribed to V—O—V (600–800 cm^{-1}) and V=O (800–1000 cm^{-1}) stretching modes in polyvanadate species, which are attributed to typical bond vibrations of VO_x [36,37]. Similar assignments were also reported on V_2O_5/TiO_2 [38,39]. Note that these assignments are also applicable to vanadium species in magnesium vanadates [31], and therefore the possible formation of such compounds could not be ruled out. For the spent catalysts (Fig. 2b), the bands in 600–1000 cm^{-1} region become very weak. Combining this observation with the XRD results (Fig. 1b), it confirms that V_2O_5 could be transformed to some new surface species which are not sensitive to Raman spectroscopy.

The properties of the catalysts were further characterized by FTIR spectroscopy and the results are shown in Fig. 3. The MgF_2 shows weak bands at 936 and 1010 cm^{-1}, which are probably due to the existence of impurity. For the fresh V_2O_5/MgF_2 catalysts (Fig. 3a), a new band at 960 cm^{-1} is observed on the $1.0V_2O_5/MgF_2$. This band (at 960 cm^{-1}) reaches the highest intensity on the $3.1V_2O_5/MgF_2$ and then decreases on the $6.4V_2O_5/MgF_2$ (even disappears on the $9.9V_2O_5/MgF_2$). This band is ascribed to the V=O band in the environment of the fluoride ions covered on the MgF_2 surface at low vanadium loading [40]. For the $6.4V_2O_5/MgF_2$ and $9.9V_2O_5/MgF_2$ catalysts, two new bands at 820 and 1020 cm^{-1} are respectively assigned to V-O-V bridge and V=O stretching vibrations, which are characteristic of bulk V_2O_5 [41] due to the growth of surface V_2O_5 particles at high loadings. This observation is in good agreement with the XRD results (Fig. 1a), as the diffractions of V_2O_5 oxide become stronger at high vanadium contents.

For the spent catalysts, simultaneous disappearance of the bands at 820 (δ_{V-O-V}), 960 ($\upsilon_{V=O}$) and 1020 ($\upsilon_{V=O}$) cm^{-1} and the emergence of a new band at 1000 cm^{-1} are observed, implying the possible conversion of V_2O_5 to new species, which has been readily observed in the XRD (Fig. 1) and Raman spectroscopic results (Fig. 2). Although the nature of such species remains unknown, some reasoning could be made based on these results. Considering the reaction process, the dehydrofluorination of HFC-245fa leads to the formation of HFC-1234ze and HF, and the products could react with V_2O_5 to form vanadium oxyfluoride compounds (VOF_x) via the reaction $V_2O_5 + HF \rightarrow VOF_x + H_2O$ or the reaction V_2O_5 + HFO-1234ze → VOF_x + 3,3,3-trifluoropropyne + H_2O. Indeed, fluorinated hydrocarbons could react with metal oxides to form metal fluorides. For example, Skapin and kemnitz [41] reported that Al_2O_3 could be transformed to AlF_3 via the reaction with CHF_3 at 300–350 °C. The fluorine atom in such VOF_x species is much more electronegative than the oxygen atom, which leads to a lower electron density of the vanadium atom and thus a red shift of the IR band [42–44]. Therefore, these results lead to a safe conclusion that drastic change of the catalysts surface occurs during the course of the reaction.

To further determine the oxidation states of the V species, XPS spectra were recorded. Fig. 4 shows the V 2p XPS spectra of the representative fresh and spent $3.1V_2O_5/MgF_2$ catalysts. The asymmetric V $2p_{3/2}$ peak of the fresh $3.1V_2O_5/MgF_2$ could be deconvoluted to two components at binding energies (BEs) of 515.9 and 517.2 eV, which could assigned to V^{3+} and V^{5+}, respectively [45]. The formation of V^{3+} species is probably due to the reduction of surface V_2O_5 under the XPS experiment conditions (i.e. high-vacuum and X-ray) [45]. For the spent $3.1V_2O_5/MgF_2$, the spectrum

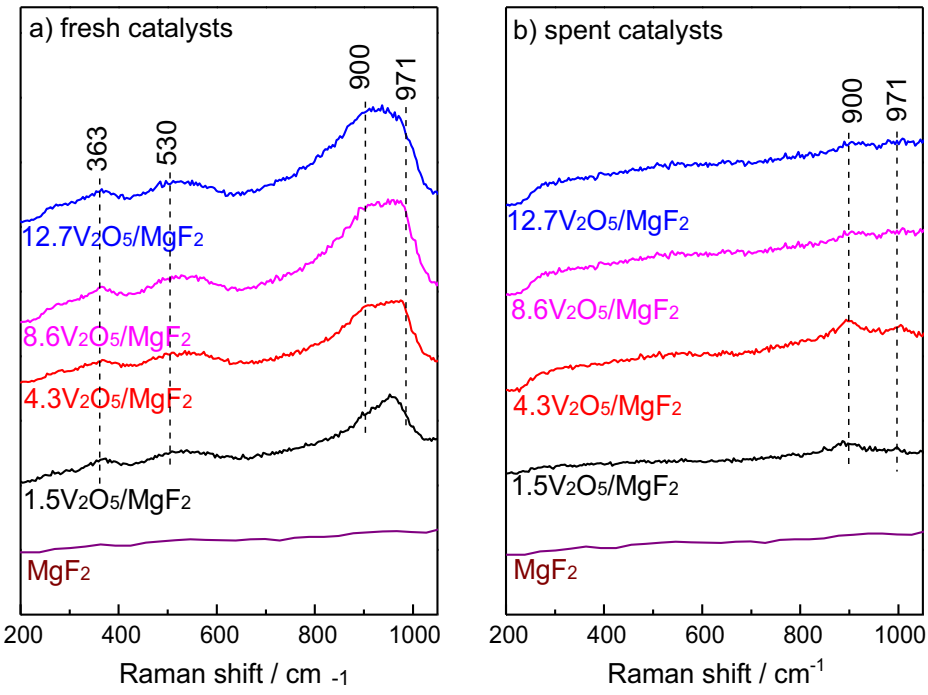

Fig. 2. Raman spectra of (a) fresh and (b) spent V_2O_5/MgF_2 catalysts.

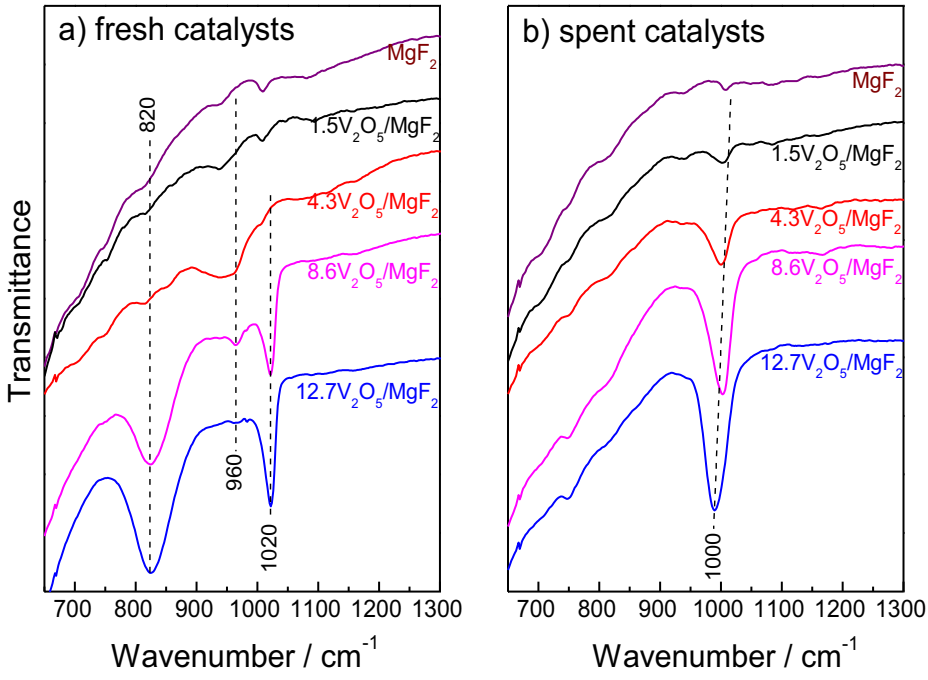

Fig. 3. FTIR spectra of (a) fresh and (b) spent V_2O_5/MgF_2 catalysts.

has similar shape as the fresh one, but obvious shift of the binding energies is observed. The V $2p_{3/2}$ peak of the spent sample could be deconvoluted to two components at binding energies of 516.4 and 517.8 eV. The shift to higher BE suggests that the electron density of the vanadium atom in the spent catalyst is lower than that in the fresh catalyst containing V_2O_5. In this case, the electron density of the vanadium atom in VOF_x specie is lower than that in the V_2O_5 due to the stronger electronegativity of the fluorine atom, which would withdraw electron from vanadium to fluorine and consequently result in higher oxidation state of the vanadium atom. Thus, the XPS results further validate the possible existence of such VOF_x species in the spent catalyst.

The surface acidity of the catalysts was measured by NH_3-TPD and FTIR spectra of pyridine adsorption, and the results are shown Fig. 5. Both the fresh and spent MgF_2 and $3.1V_2O_5/MgF_2$ catalysts show NH_3 desorption peaks in temperature range of 100–300 °C, indicating the presence weak Lewis acid sites on the catalyst surface. Moreover, quantified calculation shows that the fresh $3.1V_2O_5/MgF_2$ has higher surface acidity (14.9 μmol g^{-1}, 0.35 μmol m^{-2}) than the fresh MgF_2 (12.9 μmol g^{-1}, 0.43 μmol m^{-2}),

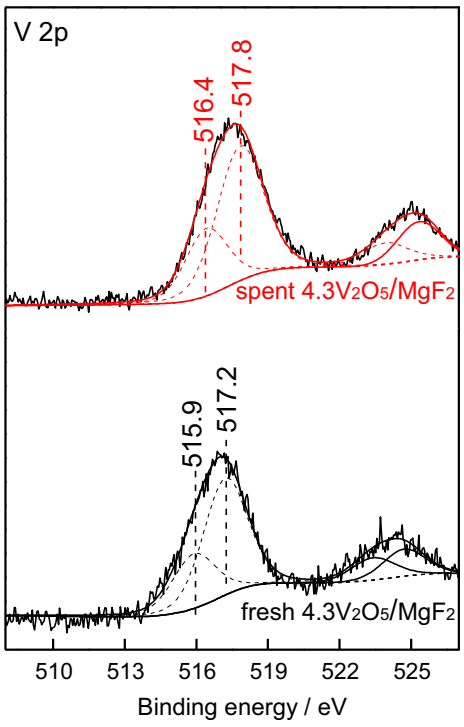

Fig. 4. XPS spectra of fresh and spent $3.1V_2O_5/MgF_2$ catalyst.

due to the additional surface acid sites provided by the V_2O_5. The spent MgF_2 has lower surface acidity (11.9 μmol g^{-1}, 0.45 μmol m^{-2}) compared to the fresh one, probably due to the coverage of surface by carbon deposit formed during the reaction . However, the spent $3.1V_2O_5/MgF_2$ has higher surface acidity (18.5 μmol g^{-1}, 0.45 μmol m^{-2}) than the fresh one, which again implies the formation of some new species possessing higher acidity than V_2O_5. Fig. 5b demonstrates the FTIR spectra of pyridine adsorption on the catalysts. All the measured catalysts show four feature bands at 1450, 1490, 1577 and 1614 cm^{-1}, which clearly indicates the presence of Lewis acid sites on the surface [46,47]. The band at 1545 cm^{-1} observed on the fresh and spent $3.1V_2O_5/MgF_2$ catalyst is assigned to Brønsted acid sites [48]. Also, the band intensities of the $3.1V_2O_5/MgF_2$ (fresh and spent) are higher than those of the MgF_2, which is consistent with the NH_3-TPD results (Fig. 5a).

3.3. Catalytic performance of V_2O_5/MgF_2 catalysts

Table 2 summarizes the surface areas, HFC-245fa conversions and HFO-1234ze selectivities of various catalysts. The supported V_2O_5/MgF_2 catalysts have higher surface areas (37.3–50.5 m^2 g^{-1}) than the MgF_2 support (30.2 m^2 g^{-1}) due to the dispersion of vanadium oxide on the MgF_2 surface. The surface areas of the spent catalysts almost remain unchanged compared to the corresponding fresh ones. The supported V_2O_5/MgF_2 catalysts have much higher activities than the MgF_2 support, highlighting the imported role of V_2O_5 in the reaction. Besides, the HFC-245fa conversion reaches an maximum (about 95%) at the catalysts containing 3.1–6.4% V_2O_5 and further increase in V_2O_5 loading results in a decline in activity. However, it should be noticed that the bulk V_2O_5 is completely inactive at 340 °C, which implies that MgF_2 is indispensable for the reaction. All the catalysts show similar selectivities (about 80% for trans-HFO-1234ze, about 20% for cis-HFO-1234ze and about 0.2% for HFO-1234yf). The intrinsic activities of the V_2O_5/MgF_2 are higher than those reported in literature. For example, the turnover frequency (TOF) of the $3.1V_2O_5/MgF_2$ at 340 °C is calculated based on its mass reaction rate (2.84 μmol s^{-1} g_{cat}^{-1}, Table 2) divided by its surface acidity (18.5 μmol g_{cat}^{-1}, Fig. 5a). The obtained TOF value (0.154 s^{-1}) is 26-fold higher than that on a $15NiO/Cr_2O_3$ catalyst (5.94×10^{-3} s^{-1} at 280 °C) in our recent work [49]. Considering that the vanadium contents in the catalysts are different, normalized specific reaction rate based on the V_2O_5 loading were also calculated. The $1.0V_2O_5/MgF_2$ catalyst has the highest specific reaction rate (134.7 μmol $s^{-1}g_{V2O5}^{-1}$) while the $9.9V_2O_5/MgF_2$ catalyst has the lowest value (18.8 μmol s^{-1} g_{V2O5}^{-1}). The XRD results (Fig. 1) show the presence of bulk V_2O_5 in the $9.9V_2O_5/MgF_2$ catalyst, thus it could be concluded that the highly dispersed vanadium

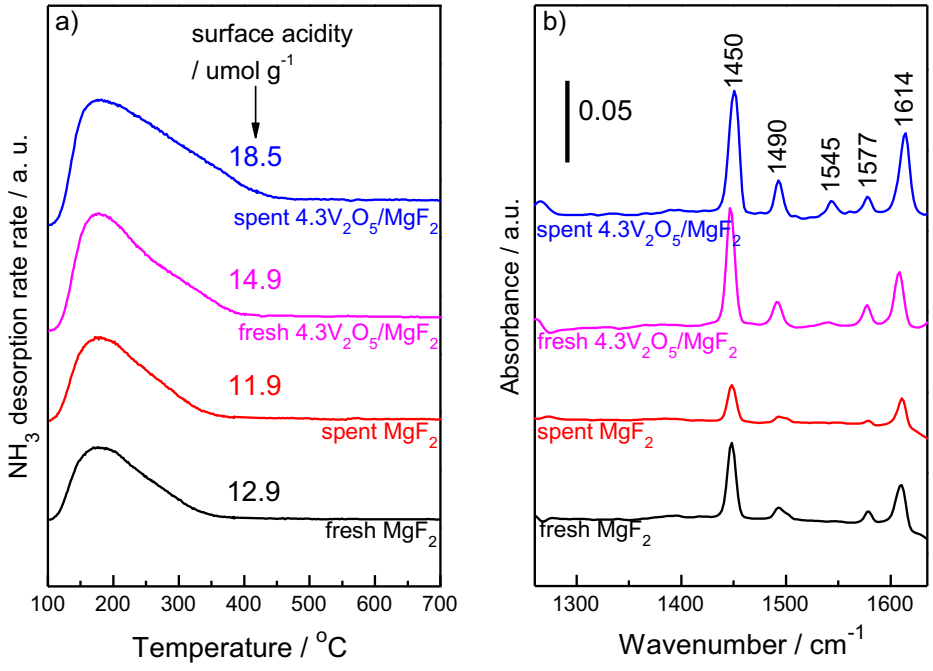

Fig. 5. (a) NH_3-TPD and (b) FTIR spectra of pyridine adsorption over fresh and spent MgF_2 and $3.1V_2O_5/MgF_2$ catalysts.

Table 2
Surface areas, HFC-245fa conversions and HFO-1234ze selectivities on V_2O_5/MgF_2 catalysts.

Catalyst	Conv.[a] /%	$S_{BET}/m^2\ g^{-1}$		Selectivity to HFO-1234ze/%		Reaction rate	
		Fresh	Spent	trans-HFO-1234ze	cis-HFO-1234ze	/μmol s^{-1} g_{cat}^{-1}	/μmol s^{-1} g_{V2O5}^{-1}
MgF_2	19.2	30.2	26.5	80.2	19.5	0.57	–
$1.0V_2O_5/MgF_2$	67.7	37.3	30.9	81.1	18.7	2.02	134.7
$3.1V_2O_5/MgF_2$	95.2	42.7	40.9	82.1	17.8	2.84	66.0
$6.4V_2O_5/MgF_2$	95.1	49.2	42.8	81.5	18.2	2.83	32.9
$9.9V_2O_5/MgF_2$	80.5	50.5	41.1	82.3	17.5	2.39	18.8
V_2O_5	0	–	–	–	–	–	–

[a] reaction temperature = 340 °C, data were taken after 1 h reaction.

species in those low-vanadium content samples are more active than the bulk ones. Many different vanadium-base catalysts have demonstrated that isolated VO_4 tetrahedral or polymeric $(VO_3)_n$ species are the catalytic active sites for oxidation, while the crystalline V_2O_5 phases possess low turnover frequencies (TOF) or expose very few active sites [50–52]. For example, Wang et al. [53] reported that the supported VO_x/Al_2O_3 showed higher activity and selectivity in comparison with bulk V_2O_5 for dehydrogenation of isobutane. Piumetti et al. [54] concluded that micro-crystalline V_2O_5 at the external surface of V-SBA-15 and V-MCF mesoporous materials were the active phase for decomposition of dichloromethane. Rodemerck et al. [55] reported that in the VO_x/MCM-41 catalysts for the non-oxidative dehydrogenation of propane and isobutane, the isolated VO_x species with stronger Lewis sites were more active than the polymeric VO_x species and crystalline V_2O_5 nanoparticles and Lewis acidic V^{3+} and V^{4+} were identified as the active sites. The important roles of highly dispersed vanadium species in oxidative dehydrogenation of propane were also illustrated by Scheurell and Kemnitz [56]. The authors prepared highly dispersed vanadium species incorporated in aluminium fluoride lattice by a modified sol - gel technique and found that the isolated vanadium species possessing large number of Lewis acid sites were responsible for the high activity and selectivity to propylene while the formed large VO_x clusters (when V content was higher than 15 mol.%) possessing Brønsted sites were responsible for the deep oxidation.

Fig. 6 shows the catalytic behaviors of the MgF_2 and $3.1V_2O_5/MgF_2$ catalysts at constant reaction temperature of 320 °C. The HFC-245fa conversion on the MgF_2 support declines from 22.0 to 10.8% after 10 h reaction. In contrast, the conversion on the $3.1V_2O_5/MgF_2$ slightly declines from 92.1% at 1 h to 90.6% at 70 h, suggesting its good stability. Moreover, an apparent induction period is observed on the $3.1V_2O_5/MgF_2$ catalyst. The conversion increases rapidly in the first 30 min (from 10 to 90%), and then it reaches a steady state. The existence of such induction period is possibly due to either the adsorption equilibrium of the reactant molecules on the catalyst surface or the formation of new active sites which can accelerate the reaction. Since there is no induction period on the MgF_2 and the content of V_2O_5 in the $3.1V_2O_5/MgF_2$ is low, it seems unlikely that the adsorption equilibrium exists because otherwise there should also be an induction period on the MgF_2. On the other hand, characterization results (Figs. 1–5) clearly suggests the possible formation of VOF_x species in the V_2O_5/MgF_2 during the reaction, which further validate the speculation that the induction period is caused by the formation of such new species. We will further discuss this point in following section based on the kinetic results. However, it should be noted that the vanadyl fluorides are volatile (i.e. VOF_3 has a melting point of 300 °C and a boiling point of 480 °C), and thus high reaction temperature should be avoided.

The catalyst deactivation during the reaction has been extensively investigated in literature and it is due to the coke deposition on the catalyst surface because of the surface acidity [57]. Fig. 7 compares the Raman spectra of the fresh and spent (after 70 h

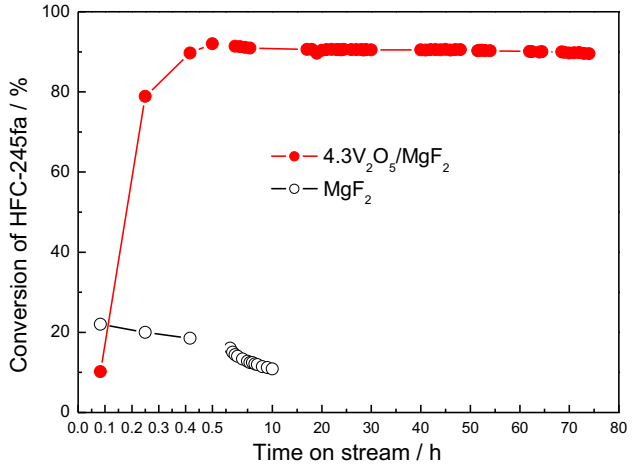

Fig. 6. Stability of MgF_2 and $3.1V_2O_5/MgF_2$ catalysts at 320 °C.

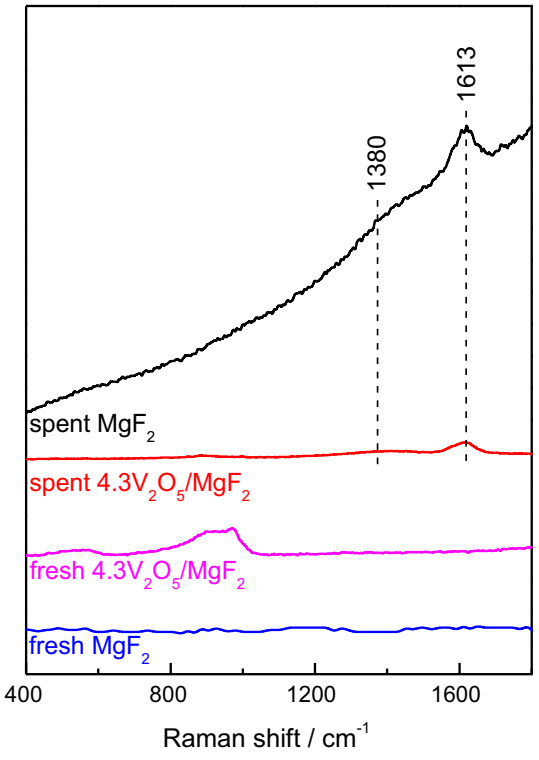

Fig. 7. Raman spectra of fresh and spent MgF_2 and $3.1V_2O_5/MgF_2$ catalysts.

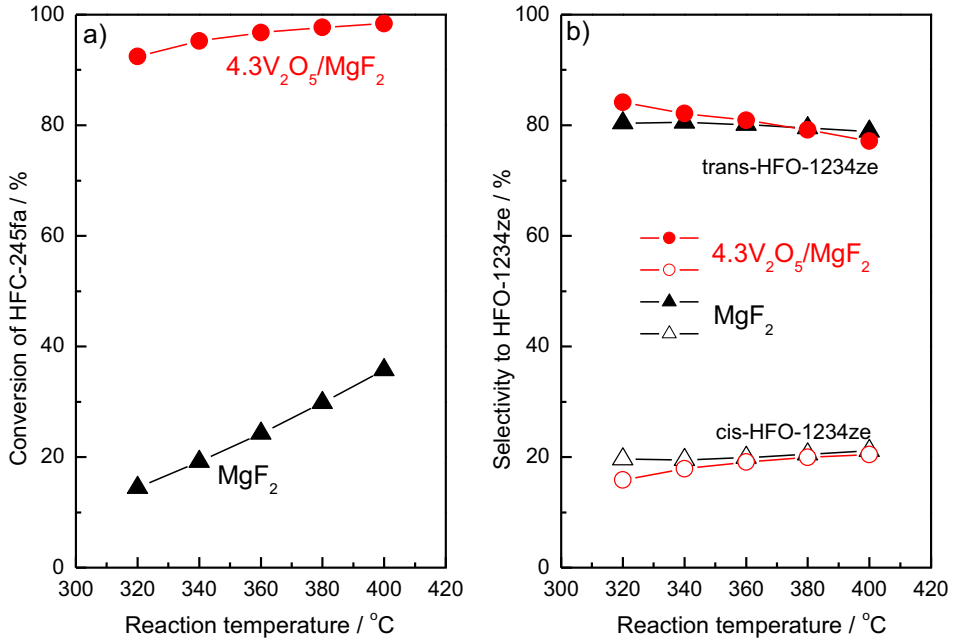

Fig. 8. (a) conversion of HFC-245fa and (b) selectivities of $3.1V_2O_5/MgF_2$ catalyst at different reaction temperatures. Space velocity = 840 h^{-1}; HFC-245fa partial pressure = 22.79 kPa. In (b), full symbols refer to selectivity to trans-HFO-1234ze and empty symbols refer to selectivity to cis-HFO-1234ze.

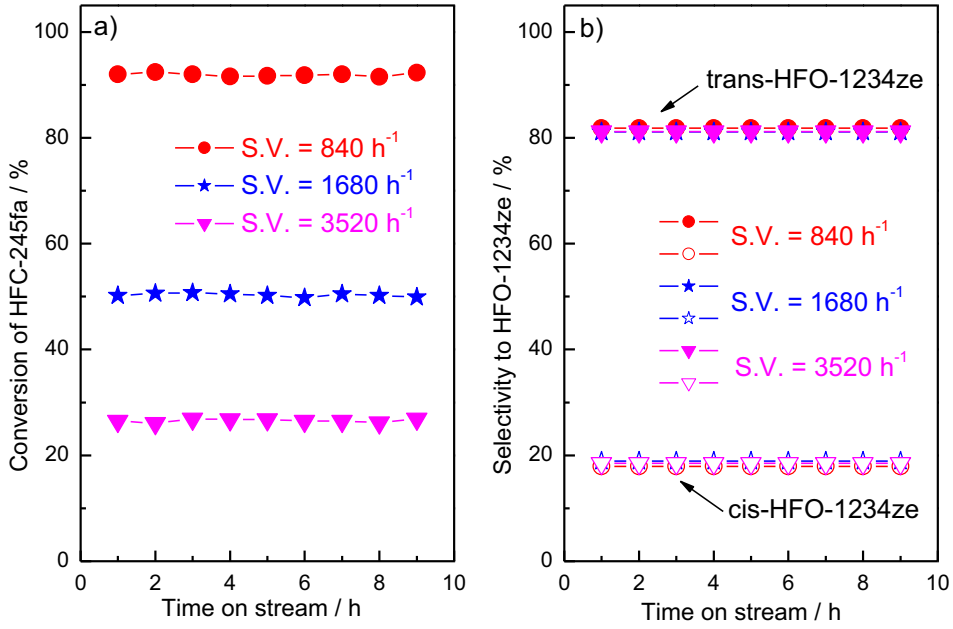

Fig. 9. (a) conversion of HFC-245fa and (b) selectivities of $3.1V_2O_5/MgF_2$ catalyst at different space velocities. Reaction temperature = 320 °C; HFC-245fa partial pressure = 22.79 kPa. In (b), full symbols refer to selectivity to trans-HFO-1234ze and empty symbols refer to selectivity to cis-HFO-1234ze.

reaction) MgF_2 and $3.1V_2O_5/MgF_2$ catalysts. It is clear that new Raman bands at 1380 and 1613 cm^{-1} are detected on the spent catalysts, which are characteristics of carbon deposition [58]. Therefore, it could be concluded that the catalyst deactivation is due to the carbon deposition on the catalyst surface during the reaction. In addition, the band intensities on the $3.1V_2O_5/MgF_2$ catalyst are much weaker than those on the MgF_2, which explains the reason that the former remains stable while the latter suffers severe deactivation.

Fig. 8 illustrates the catalytic behaviors of the MgF_2 and $3.1V_2O_5/MgF_2$ catalysts at different reaction temperatures. With the reaction temperature increasing from 320 to 400 °C, the HFC-245fa conversion on the MgF_2 gradually increases from 17 to c.a. 40%, while that on the $3.1V_2O_5/MgF_2$ increases from 91 to c.a. 99%. The selectivities remain relatively constant on both catalysts, with the selectivity to trans-HFO-1234ze being c.a. 80% while that to cis-HFO-1234ze being c.a. 20%. Also, the effect of space velocity was investigated. As shown in Fig. 9a, the HFC-245fa conversion increases from about 26% to about 90% with the space velocity decreases from 3520 h^{-1} (contact time of 1 s) to 840 h^{-1} (contact time of 3.1 s), but the calculated reaction rates remain relatively constant (2.74–3.10 μmol g_{cat}^{-1} s^{-1}). In addition, the selectivities

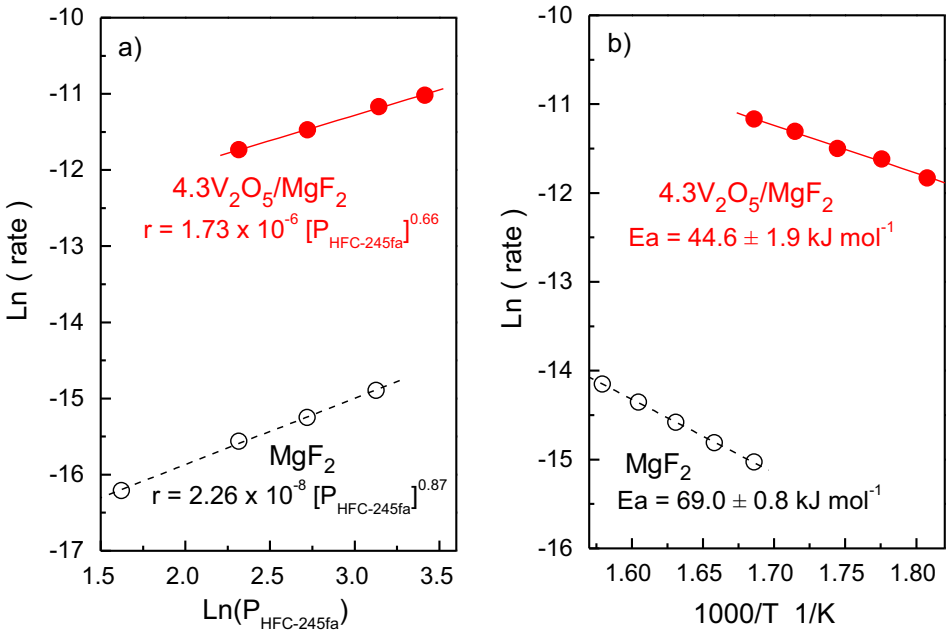

Fig. 10. (a) Dependence of reaction rates on HFC-245fa partial pressures over MgF_2 and $3.1V_2O_5/MgF_2$ catalysts and (b) Arrhenius plots of MgF_2 and $3.1V_2O_5/MgF_2$ catalysts.

Table 3
Proposed elementary steps on MgF_2 and V_2O_5/MgF_2 catalysts.

Over MgF_2 catalyst	
$CF_3CH_2CHF_2 + MgF_2 \overset{k_1}{\longleftrightarrow} CF_3CH_2CHF_2 - MgF_2$	(1)
$CF_3CH_2CHF_2 - MgF_2 \overset{k_1}{\longrightarrow} F - MgF_2 - CF_3CH_2CHF$	(2) RDS
$F - MgF_2 - CF_3CH_2CHF \overset{k_2}{\longrightarrow} CF_3CHCHF + F - MgF_2 - H$	(3)
$F - MgF_2 - H \overset{k_3}{\rightarrow} HF + MgF_2$	(4)
$CF_3CH_2CHF_2 \rightarrow CF_3CHCHF + HF$	Overall reaction
Over V_2O_5/MgF_2 catalyst[a]	
$CF_3CH_2CHF_2 + VOF_x \overset{K_1'}{\longleftrightarrow} F_3CH_2CHF_2 - VOF_x$	(1′)
$CF_3CH_2CHF_2 - VOF_x \overset{k_1'}{\rightarrow} F - VOF_x - CF_3CH_2CHF$	(2′) RDS
$F - VOF_x - CF_3CH_2CHF \overset{k_2'}{\rightarrow} CF_3CHCHF + F - VOF_x - H$	(3′)
$F - VOF_x - H \overset{k_3'}{\rightarrow} HF + VOF_x$	(4′)
$CF_3CH_2CHF_2 \rightarrow CF_3CHCHF + HF$	Overall reaction

[a] On the V_2O_5/MgF_2 catalyst, the elementary steps could include those on VOF_x and those on MgF_2. Therefore, Eqs. (1′)–(4′) only represent those steps on VOF_x.

are hardly affected by the space velocity (Fig. 9b), with the selectivity to trans-HFO-1234ze being c.a. 80% while that to cis-HFO-1234ze being c.a. 20%. The higher selectivity to trans-HFO-1234ze compared to that to cis-HFO-1234ze is due to the its much lower Gibbs free energy (i.e. −26.5 kJ mol^{-1} for the formation of trans-HFO-1234ze and −9.5 kJ mol^{-1} for the formation of cis-HFO-1234ze at 600 K), as evidenced by the thermodynamic analyses in our previous work [49]. Also, our previous analyses [49] showed that the Gibbs free energies for the reversible reactions (i.e. HFO-1234ze + HF → HFC-245fa) were +9.5 to +41.5 kJ mol^{-1} in temperature range of 600–700 K, implying that the dehydrofluorination reaction is practically irreversible. In addition, our analyses suggest that the formation of 3,3,3-trifluoro-1-propyne via dehydrofluorination of trans-/cis-HFO-1234ze would not take place because of their positive Gibbs free energies in 600–700 K region (9.0–43.5 kJ mol^{-1}) [49]. This prediction is in line with the observation in the current work as there is no 3,3,3-trifluoro-1-propyne could be detected in the products (Table 1).

3.4. Kinetic investigation

To compare the intrinsic activities of the catalysts, kinetic investigation was conducted on the representative MgF_2 and $3.1V_2O_5/MgF_2$ catalysts under differential reaction mode (with HFC-245fa conversion less than 15%) and the results are shown in Fig. 10a and Table S1. The TOFs of the catalysts under kinetic conditions were calculated. From the data taken in Table S1 (reaction temperature = 320 °C, HFC-245fa partial pressure = 22.79 kPa), the TOFs based on reaction rate (mol g_{cat}^{-1} s^{-1}) divided by surface acidity (mol g^{-1}, taken from the NH_3-TPD results in Fig. 5a) on the $3.1V_2O_5/MgF_2$ is 0.762 s^{-1}, which is 29-fold higher than that on the MgF_2 (0.026 s^{-1}). Note that the TOF (0.762 s^{-1}) on the $3.1V_2O_5/MgF_2$ is contributed from both MgF_2 and V species, and the surface acidity of this catalysts is mainly from MgF_2 (Fig. 5a), the actual TOF of the V species might be even higher. Nevertheless, the much higher TOF on the $3.1V_2O_5/MgF_2$ suggests that the reaction rate is much faster on this catalyst, most likely due to the generation of new active species. Indeed, the Arrhenius plots of the catalysts shown in Fig. 10b reveal that the activation energy of the $3.1V_2O_5/MgF_2$ (44.6 ± 1.9 kJ mol^{-1}) is much lower than that of the MgF_2 (69.0 ± 0.8 kJ mol^{-1}) (see Table S2 for detailed results), implying that the reaction route on the $3.1V_2O_5/MgF_2$ might be different from that on the MgF_2. Also, parity plots and residual analyses (Fig. S1) on these two catalysts suggest that the derived rate expressions (Fig. 10a) are valid.

It was reported in literature that dehydrofluorination [16,48] or dehydrochluorination [59] involves the cleavage of C—F (or C—Cl) and C—H bonds, which takes place on surface acid site and base site, respectively. For example, in the dehydrofluorination of 3-chloro-1,1,1,3-tetrafluorobutane over a MgF_2 catalyst, Teinz et al. [16] proposed that the 3-F atom in the reactant would interact with Mg^{2+} cation (acting as the acid site) and the neighboring H-atom would interact with the F^- anion (acting as the base site). Based on the previous findings, the elementary steps on the MgF_2 and $3.1V_2O_5/MgF_2$ catalysts are derived according to the observed kinetic results, using the classic Langmuir-Hinshelwood (L-H) model. As shown in Table 3, over the MgF_2 catalyst, the reaction sequence includes: Step 1, chemisorption of HFC-245fa molecule on the catalyst (Eq. (1)); Step

Fig. 11. Possible reaction process for dehydrofluorination of HFC-245fa over V_2O_5/MgF_2 catalysts.

2, cleavage of C—F on Mg^{2+} site (Eq. (2)). This step is the rate-determining step (RDS) because of its high C-F bond strength (about 490 kJ mol^{-1}) [48]. Step 3, sequential cleavage of C—H bond on F^- site to form the product HFO-1234ze (Eq. (3)); Step 4, formation of HF (Eq. (4)). Then the rate expression on MgF_2 could be deduced as $r_{MgF2} = k_1K_1P_{HFC\text{-}245fa}/(1 + K_1P_{HFC\text{-}245fa}) = k_{1app}P^n_{[HFC\text{-}245fa]}$, assuming that the chemisorbed HFC-245fa is the dominant surface specie. Over the $3.1V_2O_5/MgF_2$ catalyst, in addition to the steps on the MgF_2 support (Eqs. (1)–(4)), reaction could also take place on the surface VOF_x as the new active sites (V^{n+} as the acid site and F^- as the base site) and the elementary steps (Eqs. (1′)–(4′)) are similar to those on the MgF_2. The rate expression on VOF_x could be deduced as $r_{VOFx} = k'_1K'_1P_{HFC\text{-}245fa}/(1 + K'_1P_{HFC\text{-}245fa}) = k'_{1app}P^m_{[HFC\text{-}245fa]}$. Note that the reaction over the $3.1V_2O_5/MgF_2$ contains a mixture of those on MgF_2 and VOF_x, namely, $r_{3.1V2O5/MgF2} = r_{MgF2} + r_{VOFx}$, but the contribution of r_{VOFx} is much more significant than that of r_{MgF2} as the MgF_2 is much less active than the $3.1V_2O_5/MgF_2$ (Fig. 8). Thus, the expression $r_{3.1V2O5/MgF2} = r_{MgF2} + r_{VOFx}$ could be simplified to $r_{3.1V2O5/MgF2} \approx r_{VOFx} = k'_{1app}P^m_{[HFC\text{-}245fa]}$. The rate equations on the MgF_2 and $3.1V_2O_5/MgF_2$ catalysts are consistent with those based on the observed kinetics, suggesting the derived elementary steps are reasonable. Moreover, the reaction constant k_1 (or k'_1) and the adsorption equilibrium constant K_1 (or K'_1) could be deduced by linear regression, based on the rate expression $r_{MgF2} = k_1K_1P_{HFC\text{-}245fa}/(1 + K_1P_{HFC\text{-}245fa})$ or $r_{VOFx} = k'_1K'_1P_{HFC\text{-}245fa}/(1 + K'_1P_{HFC\text{-}245fa})$ and the results in Table S1 (see Fig. S2 for detailed calculation). It turns out that for the MgF_2 catalyst, the reaction constant k_1 is 1.45×10^{-6} mol g^{-1} s^{-1} and the adsorption equilibrium constant K_1 is 1.33×10^{-2} kPa^{-1}; while for the $3.1V_2O_5/MgF_2$ catalyst, the reaction constant k'_1 is 3.46×10^{-5} mol g^{-1} s^{-1} and the adsorption equilibrium constant K'_1 is 2.92×10^{-2} kPa^{-1}. On one hand, the 23-fold higher intrinsic reaction constant k'_1 (3.46×10^{-5}) on the $3.1V_2O_5/MgF_2$ than that on the MgF_2 ($k_1 = 1.45 \times 10^{-6}$ mol g^{-1} s^{-1}) suggests that the $3.1V_2O_5/MgF_2$ is much more active than the MgF_2, which is supported by its much lower Ea (Fig. 10b). The much higher rate constant of the $3.1V_2O_5/MgF_2$ may also explain the very different activities of the MgF_2 and $3.1V_2O_5/MgF_2$ catalysts despite of their practically similar surface acidity (Fig. 5a), which is due to the fact that the intrinsic activity of the VOF_x species (although in small quantity) is much higher than that of the MgF_2. On the other hand, the adsorption equilibrium constant K'_1 (2.92×10^{-2} kPa^{-1}) on the $3.1V_2O_5/MgF_2$ is two times as high as that on the MgF_2 ($K_1 = 1.33 \times 10^{-2}$ kPa^{-1}), indicating the coverage of HFC-245fa on the former catalyst is higher than that on the latter, which well explains the lower reaction order of HFC-245fa on the $3.1V_2O_5/MgF_2$ (0.66, Fig. 10a) compared to that on the MgF_2 (0.87, Fig. 10a) due to its higher amount of surface acid sites (Fig. 5a).

Based on the above results, the reaction route on the supported V_2O_5/MgF_2 catalysts could be established, as shown in Fig. 11. Considering the facts that the pure V_2O_5 is inactive and the MgF_2 gives medium HFC-245fa conversion (19.2%, Table 2), it could be deduced that the dehydrofluorination reaction first takes place on the surface of the MgF_2 support, which leads to the formation of HFO-1234ze and HF. The produced HF could react with V_2O_5 to form vanadium oxyfluoride (VOF_x), which possesses much higher intrinsic activity than MgF_2. Thus, the observed induction period on the $3.1V_2O_5/MgF_2$ catalyst (Fig. 6) could be explained as a result of MgF_2-triggered transformation of V_2O_5 to VOF_x. Moreover, it seems that the formation of such VOF_x is rather fast under the employed reaction conditions.

4. Conclusions

In summary, this work presents a study of dehydrofluorination over supported V_2O_5/MgF_2 catalysts. It is found that the addition of V_2O_5 in the MgF_2 significantly enhances both activity and stability. Such enhancement is due to the MgF_2-triggered generation of new surface VOF_x species via the reaction between V_2O_5 and HF, as evidenced by various characterization results. The kinetic investigation further demonstrates that the activation energy of the $3.1V_2O_5/MgF_2$ catalyst is much lower than that of the MgF_2, implying a different reaction route on the former catalyst. Accordingly, the proposed reaction mechanism on the $3.1V_2O_5/MgF_2$ catalyst involves an additional dehydrofluorination reaction on the VOF_x surface, which is much faster than that on the MgF_2.

Acknowledgement

This work is financially supported by the Natural Science Foundation of Zhejiang Province (No. LY17B030001), National Natural Science Foundation of China (No. 21643007 and 21773212).

Appendix A. Supplementary material

Supplementary data associated with this article can be found, in the online version, at https://doi.org/10.1016/j.jcat.2018.04.014.

References

[1] G.J. Velders, A.R. Ravishankara, M.K. Miller, M.J. Molina, J. Alcamo, J.S. Daniel, S. Reimann, Science 335 (2012) 922–923.
[2] G.J. Velders, D.W. Fahey, J.S. Daniel, M. McFarland, S.O. Andersen, Proc. Nat. Acad. Sci. 106 (2009) 10949–10954.
[3] G. Di, J.S. Nicola, L. Brown, S. Fedele, C. Zilio Bobbo, J. Chem. Eng. Data 57 (2012) 2197–2202.
[4] D.J. Luecken, R.L. Waterland, S. Papasavva, K.N. Taddonio, W.T. Hutzell, J.P. Rugh, S.O. Andersen, Environ. Sci. Technol. 44 (2010) 343–348.
[5] E. Ünveren, E. Kemnitz, A. Andreas Lippitz, W.E.S. Unger, J. Phys. Chem. B 109 (2005) 1903–1913.
[6] C.Y. Steven, F.C. David, J. Phys. Chem. B 107 (2003) 5182–5189.
[7] Y.X. Cheng, J.L. Fan, Z.Y. Xie, J.Q. Lu, M.F. Luo, J. Fluorine Chem. 156 (2013) 66–72.
[8] M. Wei, L. Kou, W. Bo, Y.B. Bai, W. Wei, J. Lu, Appl. Catal. A: Gen. 491 (2015) 37–44.
[9] K. Teinz, S.R. Manuel, B.B. Chen, A. Pigamo, N. Doucet, E. Kemnitz, Appl. Catal. B: Environ. 165 (2015) 200–208.
[10] J. He, G.Q. Xie, J.Q. Lu, L. Qian, X.L. Zhang, P. Fang, Z.Y. Pu, M.F. Luo, J. Catal. 253 (2008) 1–10.
[11] X. Zhou, P. Zhang, J. He, B. Zhou, Ind. Eng. Chem. Res. 56 (2017) 7623–7630.
[12] C.G. Krespan, V.A. Petrov, Chem. Rev. 96 (1996) 3269–3302.
[13] V.A. Petrov, C.G. Krespan, B.E. Smart, J. Fluorine Chem. 27 (1996) 139–142.
[14] E. Kemnitz, U. Gross, S. Rüdiger, C.S. Shekar, Angew. Chem. 42 (2003) 4251–4254.
[15] G.L. Li, H. Nishiguchi, T. Ishihara, Y. Moro-Oka, Y. Takita, Appl. Catal. B: Environ. 16 (1998) 309–317.
[16] K. Teinz, S. Wuttke, F. Börno, J. Eicher, E. Kemnitz, J. Catal. 282 (2011) 175–182.

[17] W. Mao, Y. Bai, B. Wang, W. Wang, H. Ma, Y. Qin, C. Li, J. Lu, Z. Liu, Appl. Catal. B: Environ. 206 (2017) 65–73.
[18] W. Jia, W. Qian, X. Lang, H. Chao, G. Zhao, J. Li, Z. Zhu, Catal. Lett. 145 (2015) 654–661.
[19] M. Wojciechowska, B. Czajka, M. Pietrowski, M. Zieliński, Catal. Lett. 66 (2000) 147–153.
[20] E. Kemnitz, Y. Zhu, B. Adamczyk, J. Fluorine Chem. 114 (2002) 163–170.
[21] J.K. Murthy, U. Gross, S. Rüdiger, E. Ünveren, W. Unger, E. Kemnitz, Appl. Catal. A: Gen. 282 (2005) 85–91.
[22] M. Nickkho-Amiry, G. Eltanany, S. Wuttke, S. Rüdiger, E. Kemnitz, J.M. Winfield, J. Fluorine Chem. 129 (2008) 366–375.
[23] Y.M. Liu, Y. Cao, N. Yi, W.L. Feng, W.L. Dai, S.R. Yan, H.Y. He, K.N. Fan, J. Catal. 224 (2004) 417–428.
[24] Y.V. Belokopytov, K.M. Kholyavenko, S.V. Gerei, J. Catal. 60 (1979) 1–7.
[25] M. Wojciechowska, W. Gut, M. Grunwald-Wyspiańska, Catal. Lett. 15 (1992) 237–245.
[26] D.H. Cho, Y.G. Kim, M.J. Chung, J.S. Chung, Appl. Catal. B Environ. 18 (1998) 251–261.
[27] B. Adamczyk, O. Boese, N. Weiher, S.L.M. Schroeder, E. Kemnitz, J. Fluorine Chem. 101 (2000) 239–246.
[28] H.S. Fogler, Elements of Chemical Reaction Engineering, Pearson Education Inc., fourth ed., 2006, pp. 839.
[29] M. Shacham, M.B. Cutlip, M. Elly. Polymath, Copyright 2006. http://www.polymath-software.com
[30] K.V. Narayana, B.D. Raju, S.K. Masthan, V.V. Rao, P.K. Rao, Catal. Lett. 84 (2002) 27–30.
[31] G. Busca, G. Ricchiardi, D.S.H. Sam, J.C. Volta, J. Chem. Soc. Faraday Trans. 90 (1994) 1161–1170.
[32] G. Liu, Z.J. Zhao, T. Wu, L. Zeng, J. Gong, ACS Catal. 6 (2016) 5207–5214.
[33] M.M. Kantcheva, K.I. Hadjiivanov, D.G. Klissurski, J. Catal. 134 (1992) 299–310.
[34] O. Ovsitser, E.V. Kondratenko, Chem. Commun. 46 (2010) 4974–4976.
[35] J. Haber, Catal. Today 142 (2009) 100–113.
[36] A. Khodakov, B. Olthof, A.T. Bell, E. Iglesia, J. Catal. 181 (1999) 205–216.
[37] C. Sanchez, J. Livage, G. Lucazeau, J. Raman Spectrosc. 12 (2010) 68–72.
[38] G.T. Went, L.J. Leu, A.T. Bell, J Catal. 134 (1991) 479–491.
[39] P. Ji, X. Gao, X. Du, C. Zheng, Z. Luo, K. Cen, Catal. Sci. Technol. 6 (2015) 1187–1194.
[40] J. Haber, J. Stoch, M. Wojciechowska, Surf. Interf. Anal. 15 (2010) 711–717.
[41] T. Skapin, E. Kemnitz, Catal. Lett. 40 (1996) 241–247.
[42] M. Mathew, A.J. Carty, G.J. Palenik, J. Am. Chem. Soc. 92 (2002) 3197–3198.
[43] C. Socolsky, S.A. Brandán, A.B. Altabef, E.L. Varetti, J. Mol. Struc.-Theochem. 672 (2004) 45–50.
[44] M.D. Zidan, A.W. Allaf, Spectrochim. Acta. A 56 (2000) 2693–2698.
[45] C. Hess, G. Tzolova-Müller, R. Herbert, J. Phys. Chem. C 111 (2007) 9471–9479.
[46] H. Choi, J.H. Bae, D.H. Kim, Y.K. Park, J.K. Jeon, Materials 6 (2013) 1718–1729.
[47] H. Lee, H.D. Jeong, Y.S. Chung, G.L. Han, M.J. Chung, S. Kim, H.S. Kim, J. Catal. 169 (1997) 307–316.
[48] M.V. Martínez-Huerta, X. Gao, H. Tian, I.E. Wachs, J.L.G. Fierro, M.A. Bañares, Catal. Today 118 (2006) 279–287.
[49] J.W. Luo, J.D. Song, W.Z. Jia, Z.Y. Pu, J.Q. Lu, M.F. Luo, Appl. Surf. Sci. 433 (2018) 904–913.
[50] F. Cavani, N. Ballarini, A. Cericola, Catal. Today 127 (2007) 113–131.
[51] I. Rossetti, L. Fabbrini, N. Ballarini, C. Oliva, F. Cavani, A. Cericola, B. Bonelli, M. Piumetti, E. Garrone, H. Dyrbeck, J. Catal. 256 (2008) 45–61.
[52] I. Rossetti, L. Fabbrini, N. Ballarini, C. Oliva, F. Cavani, A. Cericola, B. Bonelli, M. Piumetti, E. Garrone, H. Dyrbeck, Catal. Today 141 (2009) 271–281.
[53] G.J. Wang, H.C. Ma, Y. Li, Z.Y. Liu, React. Kinet. Catal. Lett. 74 (2001) 103–110.
[54] M. Piumetti, B. Bonelli, P. Massiani, S. Dzwigaj, I. Rossetti, S. Casale, L. Gaberova, M. Armandi, E. Garrone, Catal. Today 176 (2011) 458–464.
[55] U. Rodemerck, M. Stoyanova, E.V. Kondratenko, D. Linke, J. Catal. 352 (2017) 256–263.
[56] K. Scheurell, E. Kemnitz, J. Mater. Chem. 15 (2005) 4845–4853.
[57] F. Wang, W.X. Zhang, Y. Liang, Y. Wang, J.Q. Lu, M.F. Luo, Chem. Res. Chin. Univ. 31 (2015) 1003–1006.
[58] C.A. Johnson, K.M. Thomas, Fuel 63 (1984) 1073–1080.
[59] W. Mao, Y.B. Bai, W. Wang, B. Wang, Q. Xu, L. Shi, C. Li, J. Lu, ChemCatChem 9 (2017) 824–832.